

# **Thermo-Elastic and Time-Dependent Creep Evolution Behaviour of Ferritic Steel Rotating Disks using Theta Projection Concept**

**H. Daghigh\***

Young Researchers and Elite Club,  
Kashan Branch, Islamic Azad University, Kashan, Iran  
E-mail: hdaghigh@yahoo.com  
\*Corresponding author

**V. Daghigh**

Young Researchers and Elite Club,  
Jasb Branch, Islamic Azad University, Jasb, Iran  
E-mail: vahid.daghigh\_del@yahoo.com

**Received: 7 May 2017, Revised: 8 June 2017, Accepted: 17 July 2017**

**Abstract:** In this article, thermo-elastic and creep evolution behaviour of ferritic steel rotating disks with variable thickness are investigated. Four thickness profiles of uniform, convex, concave and linear are considered for the disk geometry. The material creep constitutive model is defined by the  $\Theta$  projection concept, based on the experimental results existing in the literature. Loading applied is due to the inertial body force caused by the rotation and a constant temperature field throughout the disk. To achieve history of stresses and displacements, a numerical procedure using finite difference and Prandtl-Reuss relations is used. Stress and deformation histories are calculated using successive elastic solution method. In order to verify the solution approach, both composite and aluminum rotating disks were taken into account and the thermo-elastic and time-dependent creep behaviours for composite as well as the former for aluminum were obtained. Results from the current study were found to be in very good agreement with those available from literature in the area. It was shown that convex thickness profile disks display the least creep displacement, creep effective and circumferential stresses. Additionally, constant and concave thickness profiles were positively correlated with time while for linear and convex ones, it was found to have an inverse trend.

**Keywords:** Ferritic steel rotating disks, Stress and strain redistribution, Theta projection concept, Time-Dependent creep, Variable thickness

**Reference:** Daghigh, H., Daghigh, V., “Thermo-Elastic and Time-Dependent Creep Evolution Behaviour of Ferritic Steel Rotating Disks using Theta Projection Concept”, *Int J of Advanced Design and Manufacturing Technology*, Vol. 10/ No. 3, 2017, pp. 65–79.

**Biographical notes:** **H. Daghigh** holds MSc in Rock Mechanics and is a member of Young Researchers and Elite Club in Islamic Azad University, Kashan branch. **V. Daghigh** is a PhD student in the Department of Aerospace Engineering at the Mississippi State University, USA.

## 1 INTRODUCTION

Recently, numerous researchers have directed their attention to analyse rotating disks [1-3]. This stems from both simple and complicated industrial applications. For example, in reciprocating and centrifugal compressors, aero-engines and turbojets, turbine and gas engine rotors, casting ship propellers and instruments like cover plate of rotating items, brake disks and idlers were utilized in belt assemblies [4]. Thus, taking full advantage of their capabilities based on an informed understanding of their mechanical response is of great importance. Furthermore, there are only few researchers who have focused on creep analysis and particularly time-dependent creep evolution of the rotating disks. Loghman et al., [5] studied time-dependent electro-magneto-thermo-elastic creep evolution response of rotating disks made of functionally graded piezoelectric materials (FGPM). Material properties are offered using power-law distributions in radial direction and creep parameters are also power-law functions of radius as creep constitutive model is Norton's law. History of electric potential, tangential, radial, and effective creep strain rates histories are presented. It was shown that tensile radial stress distributions lessen over the FGPM rotating disk life followed by electric potential redistributions. Hosseini Korkheili and Naghdabadi [6] proposed a semi-analytical solution for elastic analysis of functionally graded rotating disk.

In a subsequent research work, Hosseini Kordkheili and Livani [7] employed the very semi-analytical approach to study thermo-elastic creep behaviour of functionally graded rotating disk with variable thickness, considering the temperature-dependent material properties. They obtained a set of linear algebraic equations using the governing differential equations and their solutions in terms of strain rates. They found that ignoring the temperature dependency of thermal and structural properties may develop up to 200% errors in the creep analysis results. Ironically, their results were limited to the only 10.88 hours after starting creep which is not realistic in terms of component analysis. Garg et al., [8] studied the steady state creep behaviour of functionally graded disk with a linearly variable thickness and the presence of linear thermal gradient. They found that the presence of the thermal gradient may cause a drastic decrease in strain rates in comparison with those observed in the FGM disk with a constant average temperature.

Sharma et al., [9] studied the creep stresses for a thin rotating disk of exponentially variable thickness with an edge load considering Seth's transition theory. They found that edge load could relatively protect the disk against the fracture by strengthen it. Szuwalski and Ustrzycka [10] studied the influence of boundary

conditions on the optimal shape of a rotating axisymmetric annular disk leading to optimize the ductile creep rupture time. They employed finite strain theory and a physical rule by using Norton's law for generalized true stresses and logarithmic strains.

In a subsequent work, Hassani et al., [11] used semi-exact method of Liao's homotopy analysis method (HAM) and finite element method (FEM) to study stress and strain distributions of rotating disks under thermo-elasto-plastic loading conditions. They also presented a numerical solution of the governing differential based on the Runge-Kutta's method. The results of the three methods were compared and good agreement was shown. They suggested that more computation time and more computations were needed since HAM has limits in its application to problems with which other methods could readily deal. Loghman and Moradi [12] studied a smart sphere made of functionally graded piezoelectric material (FGPM) for its time-dependent creep behaviour applying internal pressure, a uniform temperature field, an electric potential, and a uniform magnetic field on the sphere. It was revealed that effective stress decreased due to applying an electric potential.

Singh [13] conducted a research work on steady state creep in a rotating disk of anisotropic aluminum silicon carbide whisker composite using Norton's power law. Stress and strain distributions were obtained for anisotropic disk and the results were compared with those for isotropic disk. While the anisotropy resulted in significant change in the strain rate, relatively small effect on the resulting stress was found. Ghorbanpour Arani et al., [14] employed a semi-analytical solution to investigate magneto-thermo-elastic response of functionally graded (FG) hollow rotating disks with variable thickness. A parabolic function of radius was utilized to portray the profile of disk thickness. The results of radial displacements and stresses for two different boundary conditions with and without the presence of magnetic field were compared for concave FG disk. They found that applying a magnetic field could diminish tensile tangential stresses.

Loghman et al., [15] studied time-dependent creep analysis of rotating disk made of Al-SiC composite using Mendelson's method of successive elastic solution. Sherby's constitutive model using Pandey's experimental results on Al-SiC composite were employed to describe the material creep behaviour. It was revealed that the solution approached to steady-state condition after nearly 50 years. Singh and Ray [16] considered an isotropic functionally graded material rotating disk with a matrix of pure aluminium in which silicon carbide particles were distributed according to the Norton's law to be investigated for its steady state creep analysis. They showed that a smaller steady state tangential and radial creep rates occurred

by approximately one magnitude of order in comparison with those in an isotropic disk having a uniform particle distribution. Eraslan and Argeso [17] used an effective numerical solution to investigate the elastic and plastic limit angular velocities for rotating disks having variable thickness in a power function form. It was found that decrease of the disk thickness at the edge and the disk mass due to the profile shape resulted in elastic and plastic limit angular velocities increase.

Hashiguchi [18] reviewed various existing constitutive equations to describe time-dependent deformation behaviour. It was shown that the plastic stretching and the creep stretching should be considered as independent quantities. Vullo and Vivio [19] considered non-linear variable thickness rotating disks subjected to thermal load for evaluation of their elastic stresses and strains. Power of linear function was used to describe thickness variation of the disk. The analytical results were compared with those available in the literature and good agreement was observed. Allam et al., [20] studied a circular elastic disk of variable thickness considering the influence of a steady coaxial current and bearing a coaxial coating. The influences of time, temperature, and rotation on the stresses and displacements were investigated using a numerical example.

Zafarmand and Hassani [21] presented elasticity solutions of two-dimensional functionally graded rotating annular and solid disks with variable thickness and axisymmetric conditions. The equations were solved using the graded finite element method (GFEM). Four different thickness profiles (constant, linear, concave and convex) and various power law exponents were considered. It was found that higher capability of angular velocity could be reached by using the variable thicknesses. Apalak and Demirbas [22] studied the thermal residual stress analyses of functionally graded clamped hollow circular plates for in-plane constant inner and outer edge heat fluxes. The material compositions varies from the pure ceramic (C) outer edge to a pure metal (M) inner edge and vice versa, that is, ceramic-to-metal or metal-to-ceramic circular plates. It was shown that a metal-rich composition led to lower normal strain levels.

Das et al., [23] carried out a research work on large-amplitude free vibration analysis of a rotating annular disk subjected to uniform axial pressure and body force due to rotation. The thickness of the disk varied exponentially. The formulation is energy-based and employs variational principles to extract the governing equations. The effects of the individual loadings and their combination on the free vibration dynamic response were presented. Recently, Alipour and Farokhi Nejad [24] studied creep behaviour characterisation of a ferritic steel alloy based on the

modified theta-projection data at an elevated temperature. Performing a series of creep-rupture tests at elevated temperature, they successfully predicted the creep-rupture behaviour using the modified three-parameter theta-projection concept. Rigorous requirements need to be met for rotating disks during operation amongst which life estimation function is of immense importance.

In order to predict the life span of rotating disks, evaluation of stress and deformation histories are a crucial contribution and therefore, time-dependent stresses and deformations histories need to be normally known in order to evade component damage and catastrophic events. To the best of the authors' knowledge, it is for the first time that thermo-elastic and time-dependent creep behaviour of ferritic steel rotating disk with variable thickness profiles are investigated using a long-term constitutive equation and semi-analytical method. In this study, a semi-analytical approach [6] is employed to investigate thermo-elastic and time-dependent creep evolution analysis of rotating ferritic steel disk with variable thickness. This method embodies the advantage of limitations removal and simplifications which are usually connected with other forms of creep analysis found in the literature. Some case studies including aluminum and composite rotating disks are used to validate the solution approach used in the present study. A simple numerical simulation using commercial finite element code ABAQUS, is also employed to validate the thermo-elastic effective stress of rotating disk with constant thickness profile.

---

## 2 MATERIAL PROPERTIES, GEOMETRY AND LOADING CONDITIONS

---

### 2.1. Material properties

The disk is made of 1/2 Cr, 1/2 Mo, 1/4 V ferritic steel with the following properties [25-26]:

Heat coefficient =  $11.7 \times 10^{-6}$  ( $1/^\circ\text{C}$ )

Poisson's ratio = 0.29, modulus of elasticity = 207 GPa

### 2.2. Geometry and loading condition

It is presumed that a thin hollow disk with constant thickness is made of ferritic steel with an inner radius  $r_i$  and outer radius  $r_o$  and radius ratio equation reference goes here  $r_o/r_i$  [15]. The disk thickness profile,  $h$ , changes radially regarding the following equation [10]:

$$h_{(r)} = h_o \left( 1 - q \left( \frac{r}{R_o} \right)^{m_1} \right), R_i < r < R_o \quad (1)$$

Where  $q$  and  $m_1$  are geometric parameters in such a way  $0 \leq q < 1$ ,  $m_1 \geq 1$  and  $h_0$  is thickness of the disk at  $r=R_i$ . To study the disk with variable thickness, different thickness profiles [4] are used which are given in Table 1. The schematic shapes of the disks are also shown by Fig. 1.

**Table 1** Different cases of thickness profiles [4]

Case (a) (Concave)	Case (b) (Linear)	Case (c) (Convex)	Case (d) (Constant)
$q \neq 0, m_1 < 1$	$q \neq 0, m_1 = 1$	$q \neq 0, m_1 > 1$	$q = 0$
$q = 0.96$	$q = 0.80$	$q = 0.4151965$	$q = 0$
$m_1 = 0.5$	$m_1 = 1.0$	$m_1 = 3.0$	-

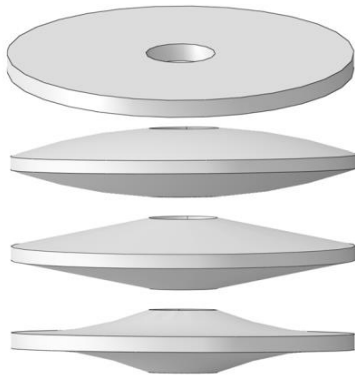


**Fig. 1** Schematic diagram of disks with constant, convex, linear and concave thickness profiles from top to bottom, respectively

The lower and upper surfaces of the disks are heat proof and without heat dispersion. The disks rotate with a constant angular velocity of  $\omega=1200$  rpm [15] making an inertia body force in a constant temperature field with temperature of  $T= 400$  °C [25-26]. A free-free condition governs the inner and outer surfaces of the disk as the boundary condition [15].

### 3 CREEP CONSTITUTIVE MODEL

The material constitutive equations indicating the material deformation under load play a pivotal role as one of the skeleton keys of inelastic analysis.

The theta  $\Theta$  projection concept is employed to enunciate the strain-time behaviour of the material with the following form [25-26]:

$$\varepsilon = \Theta_1(1 - e^{-\Theta_2 t}) + \Theta_3(e^{\Theta_4 t} - 1) \quad (2)$$

$$\dot{\varepsilon} = \Theta_1 \Theta_2 e^{-\Theta_2 t} + \Theta_3 \Theta_4 e^{\Theta_4 t} \quad (3)$$

$$\text{Log}_{10} \Theta_i = a_i + b_i T + c_i \sigma + d_i \sigma T \quad i = 1, 2, 3, 4 \quad (4)$$

Where  $T$  and  $\sigma$  represents temperature and stress levels respectively. Coefficients  $a_i$ ,  $b_i$ ,  $c_i$  and  $d_i$  are material constants. Table 2 presents these constants for this material [26]. Stress, temperature and time are represented by unites of MPa, Kelvin degree (K) and second, respectively.

**Table 2** Coefficients  $a_i$ ,  $b_i$ ,  $c_i$ ,  $d_i$  of the material constants for creep constitutive model [26]

	a	b	c	d
$\Theta_1$	-8.73	0.0046	-44.8	0.0681
$\Theta_2$	-0.00234	0.0225	0.0219	0.0000195
$\Theta_3$	-1.86	0.00203	-0.0549	0.0000799
$\Theta_4$	-16.4	0.00914	-0.0472	0.0000713

Combining equations (1) and (3) results in a set of extrapolated creep curves at different stress levels and temperatures. The full creep curves extrapolated for various stress levels are shown by Fig. 2.

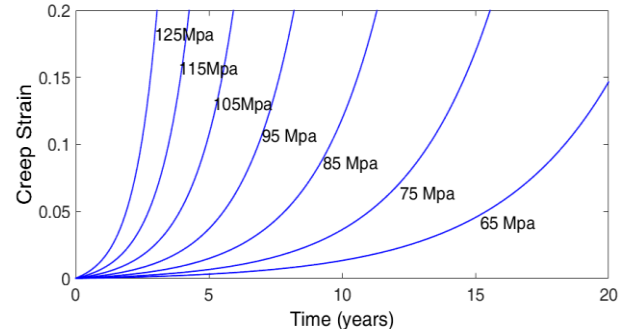


**Fig. 2** Creep curves portended by the  $\Theta$  projection concept for 1/2 Cr, 1/2 Mo, 1/4 V ferritic steel.

The current study mainly deals with the steel disk however aluminum disk [6] and composite disk [15] are also considered for validation to only verify the solution approach and formulation used in this study. This aluminum material is extracted from Ref. [6] which is FGM disk with grading index of infinity leading to a pure aluminum disk. Ref. [6] considers FGM made of aluminum as inner metal surface and zirconia as outer ceramic surface with the following properties [6]:

$$\begin{aligned}
 E_{in} &= E_{AL} = 70\text{GPa}, E_{out} = E_{Cer} = 151\text{GPa} \\
 \alpha_{in} &= \alpha_{AL} = 23 \times 10^{-6} / \text{K}, \alpha_{out} = \alpha_{Cer} = 10 \times 10^{-6} / \text{K} \\
 \rho_{in} &= \rho_{AL} = 2700\text{kg} / \text{m}^3, \rho_{out} = \rho_{Cer} = 5700\text{kg} / \text{m}^3 \\
 \nu &= 0.3
 \end{aligned}$$

Selecting grading index of zero, leads to a pure Zirconia (ceramic) disk. Increasing the grading index leads to formation of the FGM disk with a combination of ceramic and metal which finally reaches infinity grading index transforming into the pure aluminum (metal) disk. Selecting grading index to be infinity is similar to validation process chosen by Loghman et al. [5].

#### 4 THERMO-ELASTIC CREEP THEORETICAL ANALYSIS FORMULATION AND FINITE ELEMENT MODELING

##### 4.1. Overall formulation of thermo-elastic analysis

##### 4.1.1. Governing equation

Hollow axisymmetric steel disk with variable thickness is presumed. Considering the cylindrical coordinate system and the inertia body force, the equilibrium equation for axisymmetric stresses is written with the following form [15], [27]:

$$\frac{d}{dr} (h_{(r)} r \sigma_r) - h_{(r)} \sigma_\theta + h_{(r)} \rho \omega^2 r^2 = 0 \quad (5)$$

Where  $r$  is the radial coordinate,  $\sigma_r$  and  $\sigma_\theta$  are the radial and tangential stresses,  $\omega$ , the constant angular velocity,  $\rho$ , the density of the rotating disk and  $h$ , the thickness as a functional of radial coordinate.

The linear stain-displacement relationship for axisymmetric geometry and loading conditions is written as follows [27]:

$$\varepsilon_r = \frac{du}{dr}, \quad \varepsilon_\theta = \frac{u}{r} \quad (6)$$

Where  $u$  is the radial displacement,  $\varepsilon_r$  and  $\varepsilon_\theta$  are total radial and tangential strains. As an axisymmetric plane-stress problem, radial and circumferential stresses and strains may be written in terms of total strains, thermal strains and creep strains for rotating steel disks [27]:

$$\begin{cases} \varepsilon_r = \frac{1}{E(r)} (\sigma_r - \nu \sigma_\theta) + \alpha_{(r)} \Delta T_{(r)} + \varepsilon_r^c \\ \varepsilon_\theta = \frac{1}{E(r)} (\sigma_\theta - \nu \sigma_r) + \alpha_{(r)} \Delta T_{(r)} + \varepsilon_\theta^c \end{cases} \quad (7)$$

$$\begin{cases} \sigma_r = \frac{E(r)}{(1-\nu^2)} [\varepsilon_r + \nu \varepsilon_\theta - (1+\nu) \alpha_{(r)} \Delta T_{(r)} - \varepsilon_r^c - \nu \varepsilon_\theta^c] \\ \sigma_\theta = \frac{E(r)}{(1-\nu^2)} [\nu \varepsilon_r + \varepsilon_\theta - (1+\nu) \alpha_{(r)} \Delta T_{(r)} - \nu \varepsilon_r^c - \varepsilon_\theta^c] \end{cases} \quad (8)$$

Where  $\varepsilon_r$  and  $\varepsilon_\theta$  are total radial and tangential strains,  $\varepsilon_r^c$  and  $\varepsilon_\theta^c$  are radial and tangential creep strains and  $\sigma_r$  and  $\sigma_\theta$  are total radial and tangential stresses. As the Eq. (3.3) is substituted into Eq. (4.1) and then into Eq. (3.2), the Navier equation for rotating disk with variable thickness is achieved as follows:

$$\begin{aligned}
 u [ \nu E \frac{dh_{(v)}}{dr} - \frac{S_{(v)} h_{(v)}}{r} ] - (1+\nu) \alpha T_{(v)} \frac{d}{dr} [ E h_{(v)} ] - \\
 (1+\nu) E h_{(v)} r \frac{d}{dr} [ \alpha T_{(v)} ] + \varepsilon_r^c [ -r E \frac{dh_{(v)}}{dr} - (1-\nu) E h_{(v)} \\
 - h_{(v)} r \frac{dS_{(v)}}{dr} ] + \varepsilon_\theta^c [ -\nu R E \frac{dh_{(v)}}{dr} + (1-\nu) E h_{(v)} - \nu h_{(v)} r \frac{dS_{(v)}}{dr} ] \\
 - \frac{dS_r^c}{dr} [ E h_{(v)} r ] - \frac{dS_\theta^c}{dr} [ \nu E h_{(v)} r ] + (1-\nu^2) \rho h_{(v)} r^2 \omega^2 = 0
 \end{aligned} \quad (9)$$

The total strains are the sum of elastic, thermal and creep strains in Eq. (4.3). Creep strain rates are related to current stresses and the material creep constitutive model by the well-known Prandtl-Reuss equation written for plane stress condition of the disk as follows [15]:

$$\begin{cases} \dot{\varepsilon}_r^c = \frac{\dot{\varepsilon}_c}{2\sigma_e} (2\sigma_r - \sigma_\theta) \\ \dot{\varepsilon}_\theta^c = \frac{\dot{\varepsilon}_c}{2\sigma_e} (2\sigma_\theta - \sigma_r) \end{cases} \quad (10)$$

Where  $\dot{\varepsilon}_r^c$  and  $\dot{\varepsilon}_\theta^c$  are radial and tangential creep strain rates,  $\dot{\varepsilon}_c$  and  $\sigma_e$  are the effective creep strain rate and effective stress, in the order stated. Eqs. (1), (2) and (3) are used to describe the material creep constitutive model for Ferritic steel. The material creep behavior for composite disk is Sherby's constitutive model using the Pandey's experimental results on Al-SiC [21], and that for functionally graded materials is described using the Norton's law [5-6].

The von-Mises effective stress is obtained using the tangential and radial stresses through the following equation:

$$\sigma_e = \sigma_{VM} = \sqrt{\sigma_r^2 + \sigma_\theta^2 - \sigma_r \sigma_\theta} \quad (11)$$

Substituting Eq. (11) into Eq. (10), the following equation ensues [6]:

$$\begin{cases} \dot{\epsilon}_r^c = \frac{\dot{\epsilon}_c (2\sigma_r - \sigma_\theta)}{2\sqrt{\sigma_r^2 + \sigma_\theta^2} - \sigma_r \sigma_\theta} \\ \dot{\epsilon}_\theta^c = \frac{\dot{\epsilon}_c (2\sigma_\theta - \sigma_r)}{2\sqrt{\sigma_r^2 + \sigma_\theta^2} - \sigma_r \sigma_\theta} \end{cases} \quad (12)$$

**4.1.2. Boundary Conditions**

In order to satisfy the inner and outer surfaces of the free-free rotating disk, the following conditions are considered:

$$\begin{cases} \sigma_r = 0 & r = r_i \\ \sigma_r = 0 & r = r_o \end{cases} \quad (13)$$

**4.2. Solution Approach**

Since gaining a closed-form solution for ODE Eq. (9) with variable coefficients is difficult and complicated, a semi-analytical solution is endeavoured in this study. In order to reach this purpose,  $t^k$  representing the radial-width of the  $K^{th}$  sub-domain is used with which the disk is divided into some virtual sub-domains [15] displayed in Fig. 3. Where the coefficients of the Eq. (9) are considered at  $R=R(k)$ , i.e., the mean radius of the  $K^{th}$  division, an ordinary differential equation (ODE) with constant coefficients is attained.

This way, where  $m$  is the number of virtual sub-domains,  $m$  ODEs with constant coefficients are born instead of Eq. (9), a tough ODE with variable coefficients. This new set of ODEs is credible in the  $K^{th}$  sub-domain and is written with the following form :

$$C_1^k \frac{d^2 u^k}{dr^2} + C_2^k \frac{du^k}{dr} + C_3^k u^k + C_4^k = 0 \quad (14)$$

Where the coefficients are :

$$\begin{aligned} C_1^k &= r^k E h_{(r^k)} \\ C_2^k &= r^k E \left. \frac{dh_{(r)}}{dr} \right|_{r=r^k} + h_{(r^k)} E_{(r^k)} + r^k h_{(r^k)} \\ C_3^k &= \nu E \left. \frac{dh_{(r)}}{dr} \right|_{r=r^k} + \nu h_{(r^k)} - \frac{h_{(r^k)} E}{r^k} \\ C_4^k &= -(1+\nu) \alpha E T \left. \frac{d}{dr} [r^k h_{(r^k)}] \right|_{r=r^k} \\ &\quad - (1+\nu) \alpha E h_{(r^k)} r^k \left. \frac{d}{dr} [T_{(r^k)}] \right|_{r=r^k} \\ &\quad + \epsilon_r^c \left\{ -r^k E \left. \frac{dh_{(r)}}{dr} \right|_{r=r^k} - E h_{(r^k)} + \nu h_{(r^k)} E \right\} \\ &\quad - \epsilon_\theta^c \left[ -\nu r^k E \left. \frac{dh_{(r)}}{dr} \right|_{r=r^k} - \nu E h_{(r^k)} + h_{(r^k)} E \right] \\ &\quad - \frac{d \epsilon_r^c}{dr} [r^k E h_{(r^k)}] - \frac{d \epsilon_\theta^c}{dr} [\nu r^k E h_{(r^k)}] + (1-\nu^2) \rho h_{(r^k)} (r^k \omega)^2 \end{aligned} \quad (15)$$

Through finite difference method, the first and second order derivations in Eq. (14) are obtained in a way that the number of chosen sub-domains radius alters from 1 to  $n+1$ :

$$u_i' = \frac{du}{dr} = \frac{u_{i+1} - u_{i-1}}{2\Delta r} \quad (16-a)$$

$$u_i'' = \frac{d^2 u}{dr^2} = \frac{u_{i+1} + u_{i-1} - 2u_i}{\Delta r^2} \quad (16-b)$$

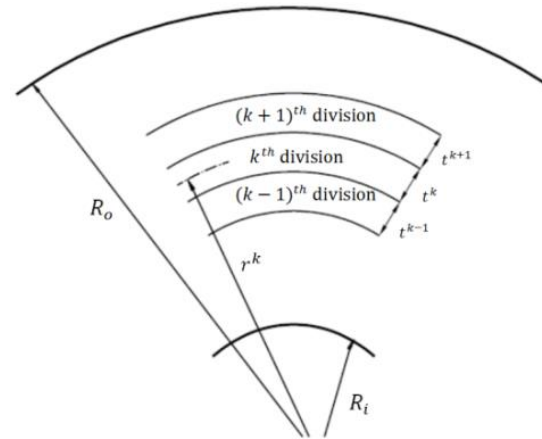


**Fig. 3** Domain divided into some finite sub-domain

It is worth noting that  $r=R_i$  when  $i=1$  and  $r=R_o$  when  $i=n+1$ . Substituting Eqs. (16-a) and (16-b) in Eq. (14) yields a matrix-form equation, i.e.

$$\underbrace{\left[ \frac{C_1(r)}{\Delta r^2} - \frac{C_2(r)}{2\Delta r} \right]}_{A(i,j-1)} u_{i-1} + \underbrace{\left[ \frac{-2C_1(r)}{\Delta r^2} + C_3(r) \right]}_{A(i,j)} u_i + \underbrace{\left[ \frac{C_1(r)}{\Delta r^2} + \frac{C_2(r)}{2\Delta r} \right]}_{A(i,j+1)} u_{i+1} = \underbrace{-C_4(r)}_{B(i)} \quad (17)$$

Where  $[A]$  is a  $(n+1) \times (n+1)$  square matrix,  $[B]$  is a  $(n+1) \times n$  column matrix, and  $A(1,1)$ ,  $A(1,2)$ ,  $B(1)$ ,  $A(n+1,n+1)$ ,  $A(n+1,n)$  and  $B(n+1)$  are attained through boundary condition in Eq.(11). Equation (17) is a matrix-form equation on the basis of displacement ( $u$ ). Subsequently, constituting  $A$  and  $B$  matrixes with the following forms resulted in obtaining the displacement:

$$u = A^{-1} \times B \quad (18)$$

Finally, the solution goes forward with the following algorithm:

- 1- Since an appropriate time step increase needs to be selected, a year is chosen for time step at  $i$ th timing  $\Delta t = 1 \text{ year}$ . The creep process goes forwards during the time and therefore, the total time is calculated through time increase summation. The total time for the  $i$ th time step is obtained with the following equation:

$$t_i = \sum_{k=1}^{i-1} \Delta t_k + \Delta t_i \quad (19)$$

2-  $\Delta \varepsilon_{\theta,ij}^c = +0.0001$   $\Delta \varepsilon_{r,ij}^c = +0.0001$  The initial quantities are presumed as  $\Delta \varepsilon_{r,ij}^c = -0.0001$  and  $\Delta \varepsilon_{\theta,ij}^c = +0.0001$  at all division points ( $j$ ) for  $i_{th}$  time step. The above initial quantities are then added to the accrued creep strains obtained from the previous time step at entire division points throughout the radius of the disk.

$$\begin{cases} \varepsilon_{r,ij}^c = \sum_{k=1}^{i-1} \Delta \varepsilon_{r,kj}^c + \Delta \varepsilon_{r,ij}^c \\ \varepsilon_{\theta,ij}^c = \sum_{k=1}^{i-1} \Delta \varepsilon_{\theta,kj}^c + \Delta \varepsilon_{\theta,ij}^c \end{cases} \quad (20)$$

It is worth noting that the incompressibility condition is considered in order for attaining creep strain escalations in axial direction.

- 3-  $\frac{d\varepsilon_r^c}{dr}$  and  $\frac{d\varepsilon_{\theta}^c}{dr}$  are calculated through Eq. (16–a).
- 4-  $C_4$  is calculated through Eqs. (15).
- 5-  $u$  is calculated through Eqs. (18).
- 6-  $\varepsilon_{\theta}$  and  $\varepsilon_r$  are achieved through Eq. (6) and Eq. (16–a), respectively.
- 7-  $\sigma_r$  and  $\sigma_{\theta}$  are calculated using Eq. (8), and subsequently  $\sigma_e$  using Eq. (11).
- 8- New quantities are then achieved for creep strain escalations through Eq. (12).

$$\begin{cases} \Delta \varepsilon_{r,ij}^c = \dot{\varepsilon}_{r,ij} \Delta t_i \\ \Delta \varepsilon_{\theta,ij}^c = \dot{\varepsilon}_{\theta,ij} \Delta t_i \end{cases} \quad (16-b)$$

To reach a convergent procedure, the initial approximations and the new obtained quantities then have to be juxtaposed with. Subsequently, time goes forward one increment and the procedure is iterated for the new time increment from step 1 provided that the convergence is met. Otherwise, the new obtained quantities of creep strain increments are presumed as initial quantities ever after and the procedure is iterated from step 2 until convergence is satisfied.

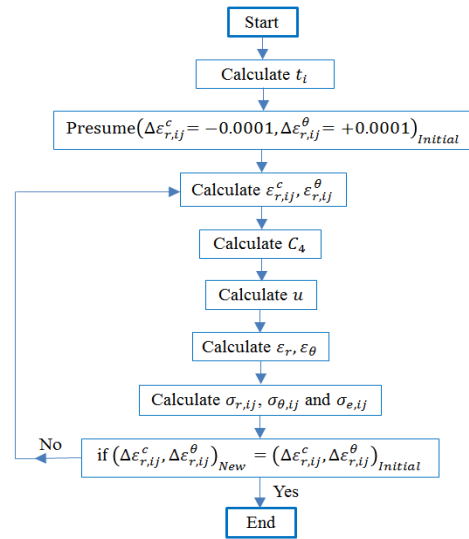


Fig. 4 A flowchart of the algorithm

It is worth to mention that  $\Delta t = 0$  in step 1 leads to initial thermo-elastic results however various non-zero  $\Delta t$  offer stresses, strains and displacements redistribution results over the time, that is, pertinent creep outputs. A flowchart of the algorithm is illustrated by Fig. 4.

### 4.3. Finite element modeling

ABAQUS is one of most popular finite element codes [28-29]. In this section, using ABAQUS finite element code, the initial thermo-elastic behavior of rotating disk with constant thickness and free-free boundary condition is studied for effective stress values. To this end, ABAQUS/Standard version 6.11, developed based on implicit solver, is employed. To mesh the rotating disk with constant thickness, free mesh technique is considered using CPS3 which is a 3-node linear plane stress triangle mesh type, as this technique matches the mesh seeds well. In this analysis, the Number of nodes and elements are 124117 and 246726, respectively. Finally, the results were obtained and then compared with those of derived by the semi-analytical solution. The difference between the two solutions is that the semi-analytical method is founded on the finite difference method, being based on derivation whilst the finite element method is based on integration. The purpose of comparison, in a sense, is to further examine the reliability of the presented semi-analytical method.

## 5 RESULTS AND DISCUSSION

Figs. 5a, b, c and d depict the initial thermo-elastic and time-dependent non-dimensional creep displacements for up to 40 years which are calculated utilizing the procedure expressed earlier for the constant, linear, concave and convex profiles of Ferritic steel rotating

disks, respectively. As can be seen, disk with constant thickness has the highest overall magnitudes of displacement amongst other types of thickness profiles mentioned in this study. The second highest overall magnitudes are related to linear profile which is slightly less than that of constant thickness. In addition, the disk with concave thickness shows the minimum amount of displacement. It is to be noted that all of the thickness profiles face similar deformation trends during the creep. First, the non-dimensional displacement diagrams linearly increase from inner surface to outer surface. Second, the rate of displacement accelerates over time, that is, the difference between 40-year and 30-year creep is much more than that of for between initial elastic and 10 year-creep. The four-part, as shown in Fig. 5, constant and concave thickness profiles experience an increasing creep rate whereas the linear and convex thickness profiles surprisingly experience a decreasing rate of creep displacement over time.

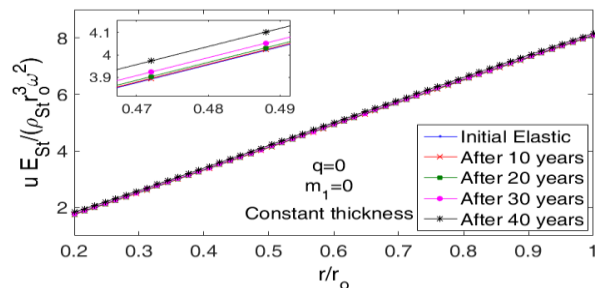


Fig. 5a Non-dimensional displacement of Ferritic steel rotating disk with constant thickness.

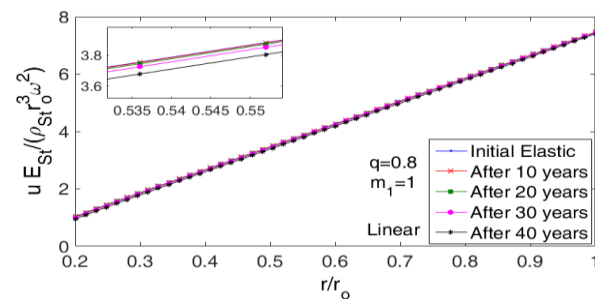


Fig. 5b Non-dimensional displacement of Ferritic steel rotating disk with linear thickness.

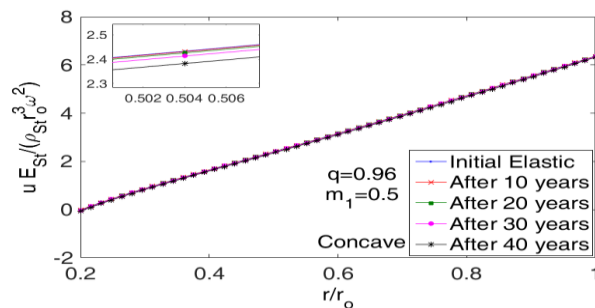


Fig. 5c Non-dimensional displacement of Ferritic steel rotating disk with concave thickness.

The circumferential radial strains redistributions for non-dimensional initial thermo-elastic and time-dependent creep up to 40 years are illustrated by Figs. 6a, b, c and d. As it is shown, all thickness profiles experience similar rate of increase in the circumferential creep strains up to 20 years. Nonetheless, the strains for different thickness profiles show a slight difference when the creep time reaches the 30-year boundary. This difference is intensified after 10-year time-lapse when a 40-year creep occurs. It can be estimated from the four-part Fig. 6 that the minimum circumferential creep strain magnitude belongs to constant thickness profiles where  $r/r_o$  is approximately 0.6.

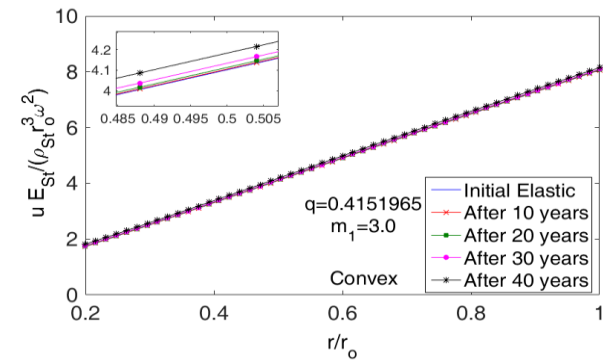


Fig. 5d Non-dimensional displacement of Ferritic steel rotating disk with convex thickness.

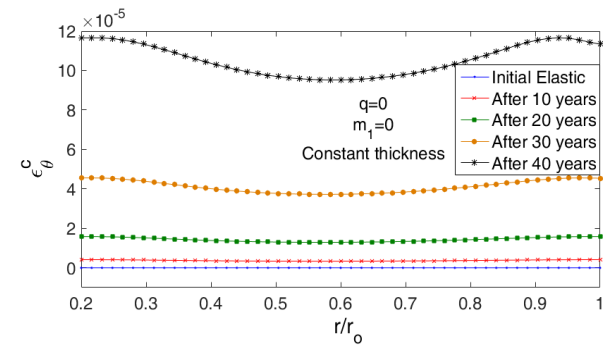


Fig. 6a Circumferential creep strain of Ferritic steel rotating disk with constant thickness.

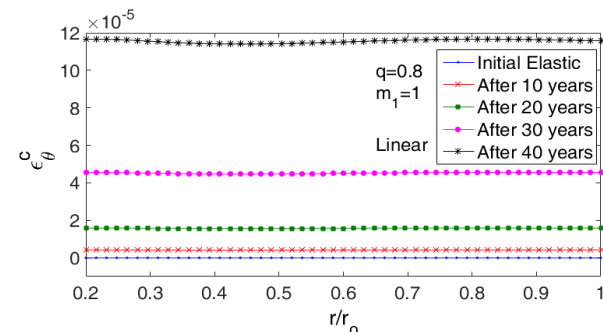


Fig. 6b Circumferential creep strain of Ferritic steel rotating disk with linear thickness profile.

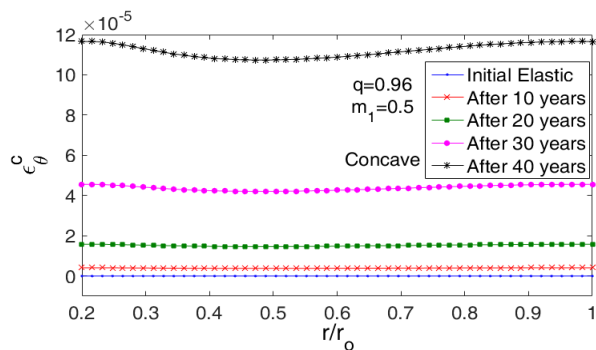


Fig. 6c Circumferential creep strain of Ferritic steel rotating disk with concave thickness profile.

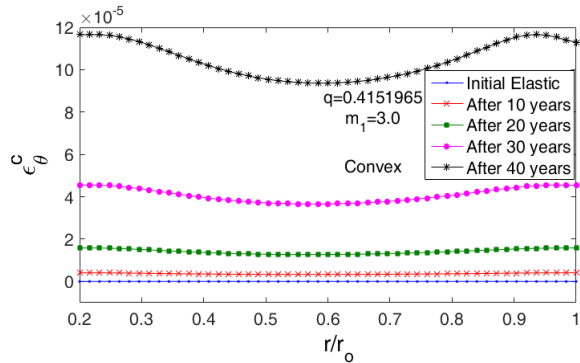


Fig. 6d Circumferential creep strain of Ferritic steel rotating disk with convex thickness profile.

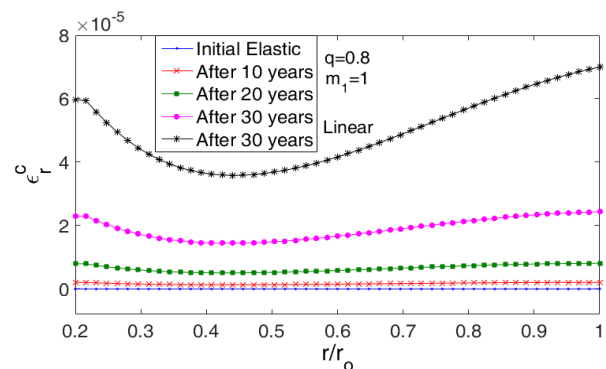


Fig. 7b Radial creep strain through the radius of hollow disk with linear thickness

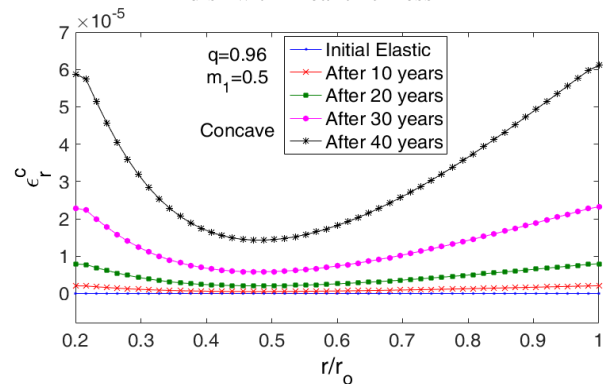


Fig. 7c Radial creep strain through the radius of hollow disk with concave thickness.

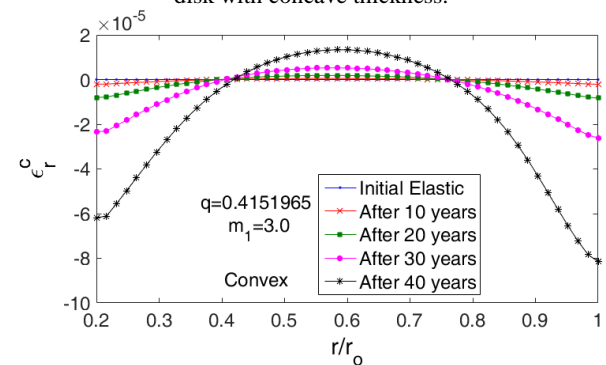


Fig. 7d Radial creep strain through the radius of hollow disk with convex thickness profile.

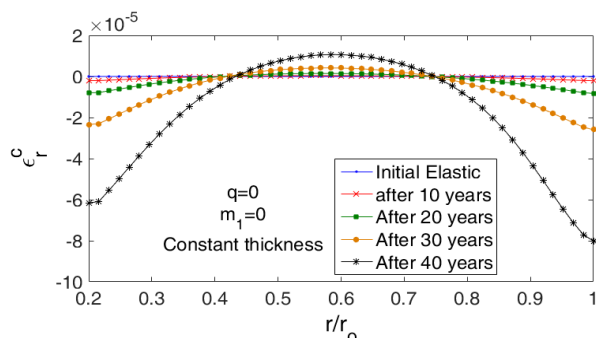


Fig. 7a Radial creep strain through the radius of Ferritic steel hollow disk with constant thickness

Fig. 7a shows the non-dimensional thermo-elastic and time-dependent radial creep strains up to 40 years. As predicted, the 40-year radial creep is dominant as opposed to shorter time intervals. It is apparent from the Fig. 7a that the 40-year radial creep reaches a peak where  $r/r_o$  is nearly 0.6.

Fig. 7b depicts the thermo-elastic and time-dependent radial creep strain up to 40 years for linear thickness profile. As shown, the 40-year radial creep experiences the highest overall magnitude in comparison with the other time intervals. It is also illustrated in the figure that the 40-year radial creep strain takes a dive where the  $r/r_o$  is nearly 0.43.

Fig. 7c and d depict the thermo-elastic and time-dependent creep behaviour of rotating disks with concave and convex thickness profiles respectively. It is clear from the Fig. 7c that the 40-year creep radial strain decreases rapidly from the inner radius to nearly  $r/r_o = 0.48$  where the creep strain goes to a minimum and then increases rapidly to reach the highest magnitude at the outer radius. Such drastic changes are considerably smaller for shorter creep time intervals. It can be seen from the Fig. 7d that the 40-year creep strain experiences the biggest positive magnitude where  $r/r_o = 0.6$  whereas the biggest negative magnitude exists at the outer surface.

Comparing Figures 6a to c shows that the constant thickness profile offers the least overall radial creep strain amongst the other thickness profiles. Similar to the creep displacements and creep circumferential strains, the magnitudes of creep radial strains tend to show a dramatic increase rate over time. Figures 8a, b, c and d describe the non-dimensional thermo-elastic and time-dependent creep circumferential stresses up to 40 years for disks with constant, linear, concave and convex thicknesses profiles, respectively. According to the four-part figure 8, the disk with convex thickness profile suggests the minimum amount of circumferential thermo-elastic and creep stress compared with the other thickness profiles. The disk with constant thickness profile however experiences the similar amounts of circumferential stress or a little more. This is while the linear thickness profile experiences the circumferential stress approximately as three-fold as those experienced by constant and convex thickness profiles. Moreover, the concave thickness profile experiences the highest magnitudes of circumferential stresses from inner to outer surface of the disks, for they are about six times more than those by constant and convex profiles. Nonetheless, the disk with concave thickness profile shows itself to great advantage over the other profiles.

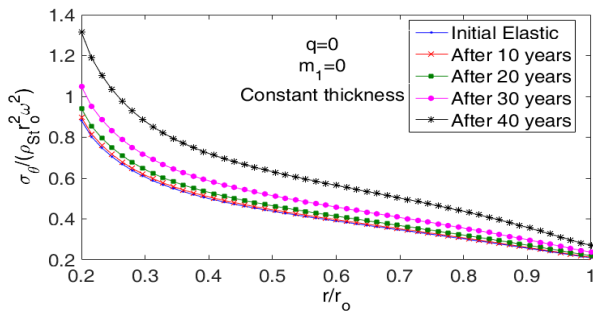


Fig. 8a Normalized circumferential creep stress through the radius of hollow disk with constant thickness profile.

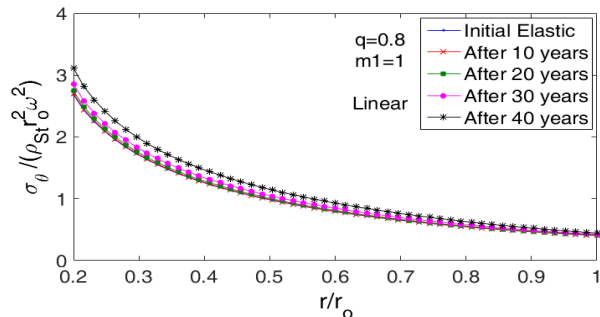


Fig. 8b Normalized circumferential creep stress through the radius of hollow disk with linear thickness profile.

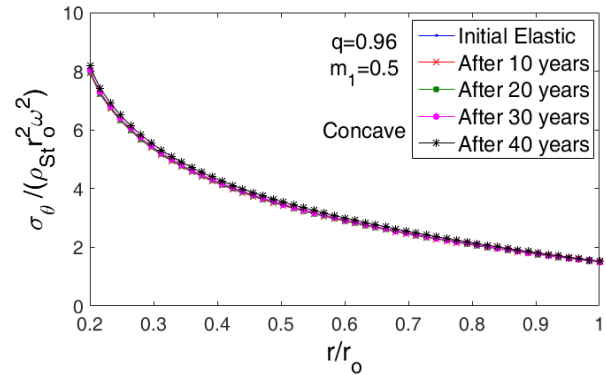


Fig. 8c Normalized circumferential creep stress through the radius of hollow disk with concave thickness profile.

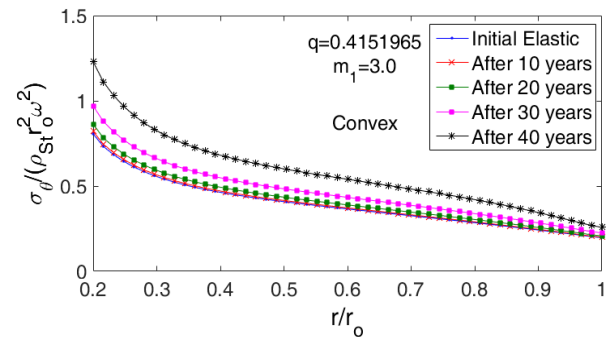
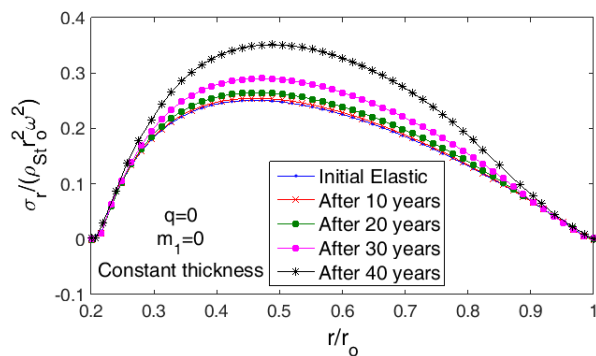


Fig. 8d Normalized circumferential creep stress through the radius of hollow disk with convex thickness profile.

The circumferential strains increase rapidly during the 40-year creep time in the disks with the constant and convex thickness profiles by approximately 50% and the one with possessing linear thickness profile by approximately 40%, whereas the disk with concave thickness profile experiences just a marginal increase by less than 5%. It may be concluded therefore that the disks with concave thickness profiles show the least effect for each time-steps in comparison with the other thickness profiles presented in this study.

Figs. 9a to d express the radial creep stress from initial elastic up to 40 years for disks with constant, linear, concave and convex thickness profiles. As the four-part Fig. 9 shows, the highest magnitude of thermo-elastic and creep radial stresses belongs to convex thickness profile. It reaches the pick where  $r/r_0$  is around 0.38. Fig. 9a illustrates that the maximum radial stresses for constant, linear and convex thickness profiles are about  $r/r_0=0.48$  and  $r/r_0=0.38$ , and  $r/r_0=0.49$ , respectively.



**Fig. 9a** Normalized radial creep stress through the radius of hollow disk with constant thickness profile.

According to the four-part Fig. 9, the non-dimensional radial stress for all thickness profiles increase with an increasing rate in a way that the difference between the initial elastic at zero time and the 30-year time period is less than the that of between 30-year and 40-year time periods. However, the sequence of these stresses becomes reverse over time when the radius ratio is more than 0.9 for concave, convex and linear thickness profiles. In fact, the 40-year creep radial stress is less than even the initial elastic radial stress. Nonetheless, the constant thickness profile does not experience such a situation. It is in agreement with what was previously observed for non-dimensional time-dependent radial stresses of rotating composite Al-Sci disk with constant thickness profile [15] in the literature as the composite disk creep radial stresses for all time periods increase across the disk. It is also a complete contrast to what was observed for non-dimensional creep radial stress of functionally graded piezoelectric rotating disks [5]. It is worthy of note that creep radial stress for ferritic steel rotating disks with all thickness profiles increases over time.

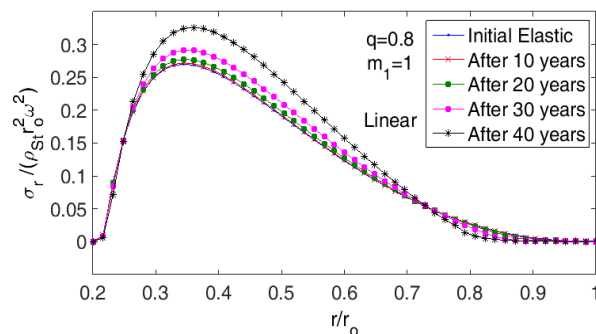


**Fig. 9b** Normalized radial creep stress through the radius of hollow disk with linear thickness profile.

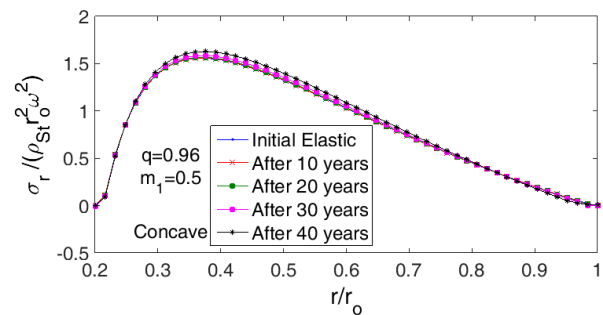


**Fig. 9c** Normalized radial creep stress through the radius of hollow disk with concave thickness profile.

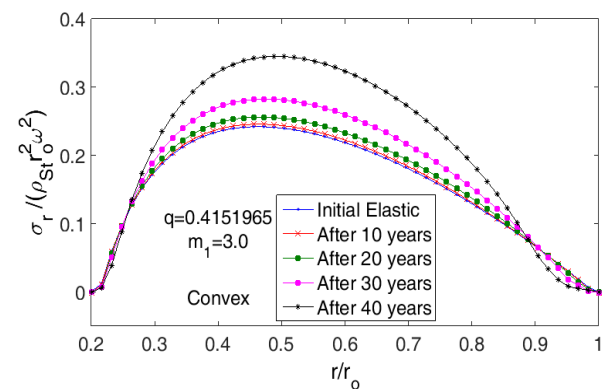


**Fig. 9d** Normalized radial creep stress through the radius of hollow disk with convex thickness profile.

The composite disk made of Al-Sci with constant thickness experiences the similar manner while the functionally graded piezoelectric rotating disk with constant thickness experiences the reverse one as the creep radial stress decreases over time [5, 15]. Creep radial stresses show high dependency on materials properties of rotating disks with time-dependent creep behaviours.

Figs. 10a to d express the effective creep stresses for the constant, linear, concave and convex thickness profiles, respectively. This four-part figure clearly shows that the general manners of effective stresses are so similar to the circumferential stresses indicating the major role of circumferential stress and negligible role of radial stress in effective stress formation. The four-part Fig. 10 illustrates that the sequence of effective creep stresses does not change during time. The initial elastic experiences the least and the 40-year creep effective stresses experience the maximum amounts from inner to outer surfaces. This is while this sequence is reverse in comparison with what previously were observed for Al-Sic composite and functionally graded piezoelectric rotating disks since the creep effective stresses sequences become reverse where the radius ratios are approximately 0.6 and 0.36, respectively.

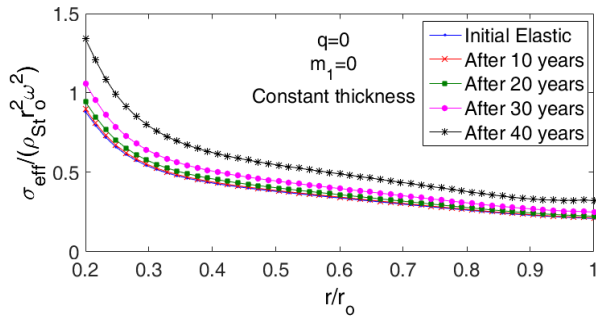


Fig. 10a Normalized effective creep stress through the radius of hollow disk with constant thickness profile.

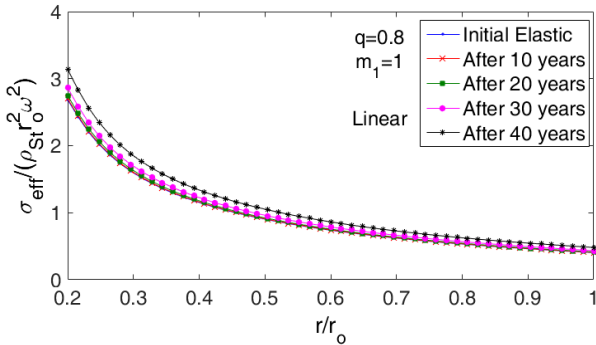


Fig. 10b Normalized effective creep stress through the radius of hollow disk with linear thickness profile

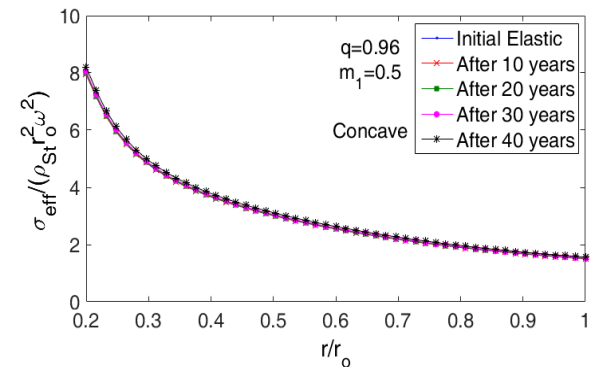


Fig. 10c Normalized effective creep stress through the radius of hollow disk with concave thickness profile.

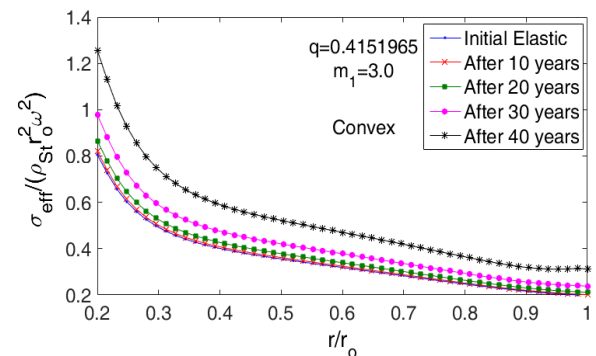


Fig. 10d Normalized effective creep stress through the radius of hollow disk with convex thickness profile.

As far as the authors know, thermo-elastic and time-dependent creep behaviour of rotating disks with various thickness profiles made of ferritic steel have not yet presented in the published literature. However, thermo-elastic behaviours of rotating disks made of functionally graded materials [5, 6] and time-dependent creep analysis of composite rotating disk made of Al-SiC [15] both with constant thickness profiles, are available in the literature. In order to confirm and validate the solution approach offered in this study, the identical materials properties as well as the same boundary conditions mentioned in the above references are considered for comparison. The FGM non-dimensional initial elastic radial stress with constant thickness profile [5-6] and history of non-dimensional creep effective stress for composite constant thickness profile disk from initial elastic up to 30 years [15] are calculated and compared with the data available in the mentioned references. Figs. 10a and b illustrate the comparisons between the results in the order stated. In general, good agreements are observed in all cases. In addition, the initial elastic effective stress for Ferritic steel rotating disk with constant thickness profile possessing the outer radius of 1 and inner radius of 0.2 meter is calculated and compared with the results obtained by commercial finite element modeling code ABAQUS.

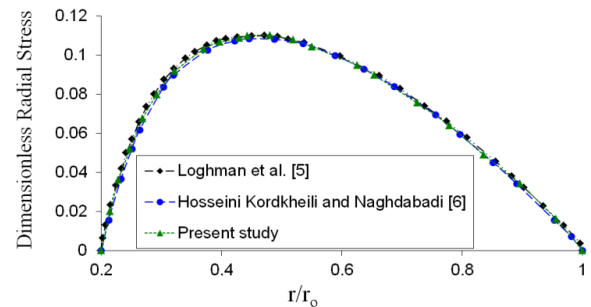


Fig. 11a Comparison of the normalized radial stress versus dimensionless radius for functionally graded materials rotating disks with constant thickness profile between present work and Refs. [5-6]

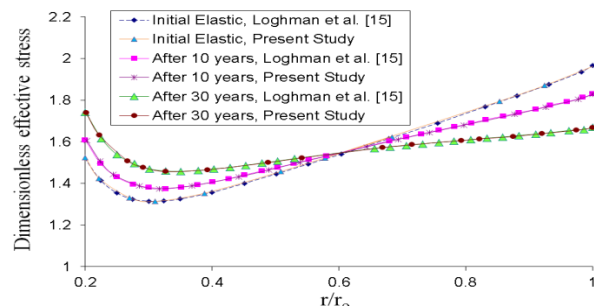
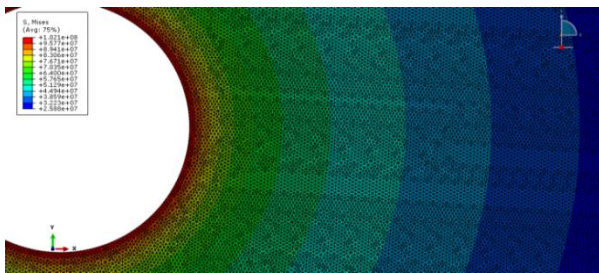
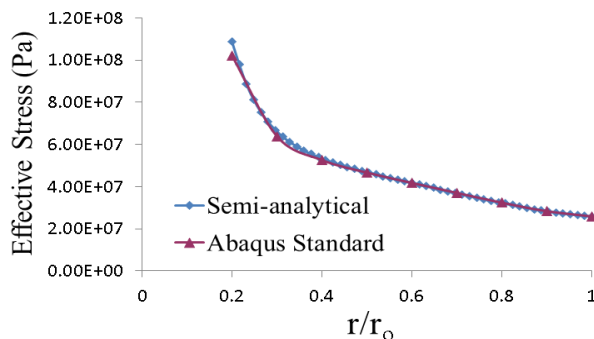


Fig. 11b Comparison of the normalized effective stress versus dimensionless radius for composite materials rotating disk with constant thickness profile between present work and Ref. [15].



**Fig. 11c** Effective stress contour for rotating disk with constant thickness profile with high magnification at the inner radius.

Fig. 11c illustrates the effective stress contour with high magnification at the inner radius. Also, Fig. 11d shows the comparison between the FEA and semi-analytical results, which a good agreement is found. As it is clear from Fig. 11c, the maximum discrepancy is 6% at the inner radius and that is less than 1% for the points where the radius ratio is more than 0.3.



**Fig. 11d** Comparison of the normalized effective stress versus dimensionless radius for composite materials rotating disk with constant thickness profile between present work and FEA.

## 6 CONCLUSIONS

In the present research work, for the first time, rotating hollow disks made of ferritic steel with various thickness profiles, namely linear, convex and concave shapes as well as constant thickness were studied for their thermo-elastic and time-dependent creep behaviour. Their radial and circumferential stresses, and displacements as well as circumferential stresses over the time, from zero up to 40 years have been analysed. In order to validate the solution approach, the results for thermo-elastic solution and time-dependent creep behaviour of aluminum and composite materials were calculated and compared with those available in the existing literature. A reasonable agreement was shown between the results. In addition, a simple simulation for thermo-elastic effective stress of Ferritic steel with a constant thickness profile was carried out using commercial finite element code ABAQUS and a good agreement was observed. The results for Ferritic

steel disk were also compared with those of composite Al-Sic and functionally graded piezoelectric disks available in the literature. The comparison indicates that material properties itself play a key role in time-dependent creep behaviours. The results obtained are concluded as:

- 1- Rotating hollow disks with convex thickness profile show the smaller amount of creep displacement, creep effective and circumferential stresses in comparison with constant, linear and concave thickness profiles.
- 2- General behaviour of effective stresses is very similar to the circumferential stresses indicating the major role of circumferential stress and a negligible role of radial stress in effective stress formation.
- 3- Normalized creep displacements increase over time for constant and concave thickness profiles whereas they decrease for linear and convex thickness profiles.
- 4- Creep radial stresses for ferritic steel rotating disks increase over time and it is in agreement with previously observed results for non-dimensional time-dependent radial stresses of rotating composite Al-Sic disk with constant thickness profile, because the composite disk creep radial stresses for all time periods increase across the disk. It also shows a reverse trend as compared with the results observed for non-dimensional creep radial stress of functionally graded piezoelectric rotating disks.
- 5- The sequence of creep radial stresses of ferritic steel disks with all thickness except for constant profiles become reverse when the radius ratio is more than 0.9. Therefore, the creep radial stresses for ferritic steel disk with constant thickness profile increase over time and throughout the disk and it is congruent with those results for composite disk made of Al-Sic. This is also in contrast to those for piezoelectric rotating disk with constant thickness profile in the literature.
- 6- The disk with concave thickness profile displays the highest circumferential and consequently effective stresses in comparison with the constant, linear and concave thickness profiles. However, it shows the least amount of impressionability for circumferential and effective stress changes over the creep time.

## REFERENCES

- [1] Loghman, A., Azami, M., "A Novel Analytical-Numerical Solution for Nonlinear Time-dependent

- Electro-thermo Mechanical Creep Behavior of Rotating Disk Made of Piezoelectric Polymer”, *Applied Mathematical Modelling*, Vol. 40, 2016, pp. 4795–4811.
- [2] Daghigh, V., Daghigh, H., Loghman, A., and Simoneau, A., “Time-dependent Creep Analysis of Rotating Ferritic Steel Disk using Taylor Series and Prandtl–Reuss Relation”, *International Journal of Mechanical Sciences*, Vol. 77, 2013, pp. 40–46.
- [3] Deepak, D., Gupta, V. K., and Dham, A. K., “Creep Modeling in Functionally Graded Rotating Disc of Variable Thickness”, *Journal of Mechanical Science and Technology*, Vol. 24, 2010, pp. 2221–2232.
- [4] Bayat, M., Saleem, M., Sahari, B. B., Hamouda, A. M., and Mahdi, E., “Analysis of Functionally Graded Rotating Disks with Variable Thickness”, *Mechanics Research Communications*, Vol. 35, 2008, pp. 283–309.
- [5] Loghman, A., Abdollahian, M., Jafarzadeh Jazi, A., and Chorbanpour Arani, A., “Semi-analytical Solution for Electromagnetothermoelastic Creep Response of Functionally Graded Piezoelectric Rotating Disk”, *International Journal of Thermal Sciences*, Vol. 65, 2013, pp. 254–266.
- [6] Hosseini Kordkheili, S. A., Naghdabadi, R., “Thermoelastic Analysis of Functionally Graded Rotating Disk”, *Composite Structure*, Vol. 79, 2007, pp. 508–516.
- [7] Hosseini Kordkheili, S. A., Livani, M., “Thermoelastic Creep Analysis of Functionally Graded Various Thickness Rotating Disk with Temperature-dependent Material Properties”, *International Journal of Pressure Vessels and Piping*, Vol. 111–112, 2013, pp. 63–74.
- [8] Garg, M., Salaria, B. S., and Gupta, V. K., “Effect of Thermal Gradient on Steady State Creep in a Rotating Disk of a Variable Thickness”, *Procedia Engineering*, Vol. 55, 2013, pp. 542–547.
- [9] Sharma, S., Sahai, L., and Kuma, R., “Creep Transition of a Thin Rotating Annular Disk of Exponentially Variable Thickness with Inclusion and Edge Load”, *Procedia Engineering*, Vol. 55, 2013, pp. 542–547.
- [10] Szuwalski, K., Ustrzycka, A., “The Influence of Boundary Conditions on Optimal Shape of Annular Disk with Respect to Ductile Creep Rupture time”, *European Journal of Mechanics - A/Solids*, Vol. 37, 2013, pp. 79–85.
- [11] Hassani, A., Hojjati, M. H., Farrahi, G. H., and Alashti, R. A., “Semi-exact Solution for Thermo-Mechanical Analysis of Functionally Graded Elastic-strain Hardening Rotating Disks”, *Communications in Nonlinear Science and Numerical Simulation*, Vol. 17, 2012, pp. 3747–3762.
- [12] Loghman, A., Moradi, M., “The Analysis of Time-Dependent Creep in FGPM Thick Walled Sphere under Electro-Magneto-Thermo-Mechanical Loadings”, *Mechanics of Time-Dependent Materials*, Vol. 17, 2013, pp. 315–329.
- [13] Singh, S. B., “One Parameter Model for Creep in a Whisker Reinforced Anisotropic Rotating Disk of Al-SiCw Composite”, *European Journal of Mechanics - A/Solids*, Vol. 27, 2008, pp. 680–690.
- [14] Ghorbanpour Arani, A., Loghman, A., and Shajari, A. R., “Semi-analytical Solution of Magneto-Thermo-elastic Stresses for Functionally Graded Variable Thickness Rotating Disks”, *Journal of Mechanical Science and Technology*, Vol. 24, 2013, pp. 2107–2117.
- [15] Loghman, A., Ghorbanpour Arani, A., Shajari, A. R., and Amir, S., “Time-dependent Thermoelastic Creep Analysis of Rotating Disk Made of Al-SiC Composite”, *Archive of Applied Mechanics*, Vol. 81, 2011, pp. 1853–1864.
- [16] Singh, S. B., Ray, R., “Creep Analysis in an Isotropic FGM Rotating Disk of Al-SiC Composite”, *Journal of Materials Processing Technology*, Vol. 143–144, 2003, pp. 616–622.
- [17] Eraslan, A. N., Argeso, H., “Limit Angular Velocities of Variable Thickness Rotating Disks”, *International Journal of Solids and Structures*, Vol. 39, 2002, pp. 3109–3130.
- [18] Hashiguchi, K., “Time-dependent Elastoplastic Constitutive Equation”, *Archives of Mechanics*, Vol. 52, 2000, pp. 609–628.
- [19] Vullo, V., Vivio, F., “Elastic Stress Analysis of Non-linear Variable Thickness Rotating Disks Subjected to Thermal Load and Having Variable Density Along the Radius”, *International Journal of Solids and Structures*, Vol. 45, 2008, pp. 5337–5355.
- [20] Allam, M. N. M., Badr, R. E., and Tantawy, R., “Stresses of a Rotating Circular Disk of Variable Thickness Carrying a Current and Bearing a Coaxial Viscoelastic Coating”, *Applied Mathematical Modelling*, Vol. 32, 2008, pp. 1643–1656.
- [21] Zafarmand, H., Hassani, B., “Analysis of Two-Dimensional Functionally Graded Rotating Thick Disks with Variable Thickness”, *Acta Mechanica*, Vol. 225, 2014, pp. 453–464.
- [22] Apalak, M. K., Demirbas, M. D., “Thermal Residual Stresses in In-plane Functionally Graded Clamped Hollow Circular Plates Subjected to an Edge Heat Flux”, *Mechanical Engineers, Part L: Journal of Materials: Design and Applications*, Vol. 229, 2015, pp. 236–260.
- [23] Das, D., Sahoo, P., and Saha, K., “Dynamic Analysis of Rotating Annular Disk of Variable Thickness under Uniform Axial Pressure”, *International Journal for Computational Methods in Engineering Science and Mechanics*, Vol. 13, 2012, pp. 37–59.
- [24] Alipoura, R., Farokhi Nejad, A., “Creep Behaviour Characterisation of a Ferritic Steel Alloy Based on the Modified Theta-Projection Data at an Elevated Temperature”, *International Journal of Materials Research*, Vol. 107, 2016, pp. 406–412.
- [25] Loghman, A., Wahab, M. A., “Creep Damage Simulation of Thick-walled Tubes using  $\Theta$  Projection Concept”, *International Journal of Pressure Vessels and Piping*, Vol. 67, 1996, pp. 105–111.
- [26] Loghman A., Shokouhi N., “Creep Damage Evaluation of Thick-walled Spheres using a Long-Term Creep Constitutive Model”, *Journal of Mechanical Science and Technology*, Vol. 23, 2009, pp. 2577–2582.

- [27] Mendelson, A., "Plasticity: Theory and Application", Krieger, New York, 1983.
- [28] Daghigh, V., Soroush, M., Nikbin, K., and Simoneau, A., "Finite Element Modeling of Tensile and Bending on Fiber Reinforced Polymer Composites", The 3rd International Conference on Composites: Characterization, Fabrication and Application (CCFA-3), Tehran, 2012, pp. 197–198.
- [29] Daghigh, V., Soroush, M., Daghigh, H., and Nikbin, K., "Buckling Behavior of Basalt Fiber Reinforced Epoxy Composites-Experimental and Numerical Investigation", In: Proceeding of The Bi-Annual International Conference on Experimental Solid Mechanics, Tehran, 2014, pp. 1409-1414.